

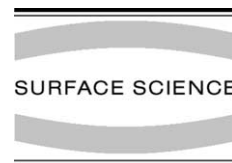


ELSEVIER

Available online at www.sciencedirect.com

SCIENCE @ DIRECT®

Surface Science 540 (2003) 285–294



www.elsevier.com/locate/susc

Scattering and recoiling mapping of the Kr–Pt(1 1 1) system by SARIS

I.L. Bolotin, A. Kutana, B.N. Makarenko¹, J.W. Rabalais^{*}

Department of Chemistry, University of Houston, Houston, TX 77204-5641, USA

Received 20 March 2003; accepted for publication 29 May 2003

Abstract

The technique of angle resolved mapping of scattering and recoiling imaging spectra (SARIS) combined with computer simulations is demonstrated to be a valuable tool for characterization of atomic collision events on surfaces. The energy distributions of scattered Kr and fast recoiled Pt atoms from a Pt(1 1 1) surface were measured as a function of exit angle. The use of a large area microchannel plate detector and time-of-flight techniques decreases the collection time and increases the number of detected trajectories above that of other designs. Classical ion trajectory simulations using the three-dimensional scattering and recoiling imaging code are used to simulate the kinematics of the scattering and recoiling particles. It is shown that SARIS mapping allows one to probe the kinematics of both scattered and recoiled particles, the probability for their occurrence in specific trajectories, their detection probabilities, and their threshold detection velocity. The measured and simulated energy distributions agree quantitatively if the detection efficiency is taken into account. The observed value of the threshold detection velocity for Pt atoms, $v^{\text{th}} = 3.78(5) \times 10^4$ m/s, is in good agreement with previous studies.

© 2003 Elsevier B.V. All rights reserved.

Keywords: Low energy ion scattering (LEIS); Computer simulations; Platinum

1. Introduction

Collisions of energetic particles with solid surfaces are of importance to many material processing and fabricating techniques. Low energy ion scattering spectrometry with time-of-flight (TOF) detection has been used extensively to study the

composition and structure of surfaces. The attractive features of this technique are its high sensitivity due to efficient detection of both scattered and recoiled ions and neutrals, the ability to detect light atoms such as hydrogen, its extreme surface sensitivity, its non-destructive nature due to the use of extremely low ion beam current densities ($\sim 10^{10}$ – 10^{11} primary ions/cm²), its sensitivity to surface structural features, and its independence of the chemical environment due to detection of both neutrals and ions. Recently developed large solid angle detection instruments for scattering and recoiling imaging spectrometry (SARIS) [1,2] provide spatial- and time-resolved,

^{*} Corresponding author. Tel.: +1-713-743-3282; fax: +1-713-743-2709.

E-mail address: rabalais@uh.edu (J.W. Rabalais).

¹ Permanent address: A.F. Ioffe, Physical-Technical Institute, Russian Academy of Sciences, St. Petersburg 194021 Russia.

element-specific images from surfaces that directly expose the three-dimensional anisotropy of keV scattered and recoiled atoms. The technique has been used for structural information, compositional analysis of surfaces, and ion fraction mapping [3–6].

Computer simulations of ion–surface collision processes have undergone extensive development in the past two decades. These simulations are a complementary source of information that provides valuable insight into the microscopic collision details. There are many benefits to the use of numerical methods in this field. The relevant collision processes can be determined, leading to a better understanding of the experiment and even the development of new experimental methods. As an example, the channeling effect originally discovered by computer simulations [7] is now used in channeling analysis techniques. They also help to determine quantities such as penetration thresholds for certain ion–target combinations, scattering and recoiling yields, collision cascade lengths, sputtering yields, etc. The recently developed scattering and recoiling imaging code (SARIC) [8,9] is a classical ion trajectory program that simulates two-dimensional scattering and recoiling patterns and provides quantitative interpretations of ion scattering and recoiling images from SARIS.

The purpose of this paper is to introduce high-precision angle-resolved mapping of scattered and recoiled particles with a large area detector, combined with computer simulations as a quantitative tool for characterization of scattering and recoiling events on surfaces. In contrast to analysis of scattering features, there have been very few studies [10–13] focused on the relationship between the kinetic energies of recoiled particles and the emission angles, which, in the azimuthal distribution of these particles, reflects the geometric structure of the surface. It is shown herein that scattering and recoiling SARIS mapping allows one to probe the kinematics of both types of emitted particles, the probability for their occurrence in specific trajectories, their detection probabilities, and their threshold detection velocity. Due to the large solid angle subtended by the microchannel plate (MCP) detector, atoms and ions

that are scattered and recoiled in both planar and non-planar directions are detected simultaneously under the same conditions. This greatly reduces the data collection time, allowing investigations of dynamic processes and phenomena that are sensitive to surface conditions, such as scattered and recoiled ion fractions.

2. Methods

2.1. Experimental methods

The experiments were performed in an ultra high vacuum chamber with a base pressure $\sim 5 \times 10^{-10}$ Torr. The system is equipped with LEED optics and a sputter ion gun for sample cleaning. All measurements were made with the sample at room temperature in a SARIS spectrometer that has been described in detail elsewhere [1–5]. Briefly, a pulsed Kr^+ beam [14] scatters and recoils atoms from the surface. The velocities of the keV ejected atoms and ions are analyzed by measuring their flight times from the sample to a rectangular position sensitive MCP detector [15] with a sensitive area of $3.5 \times 4.5 \text{ cm}^2$. The detector is gated so that it can be activated in windows of $\sim 4 \mu\text{s}$ duration that are appropriate for collection of specific scattered or recoiled atoms. The amount of information contained in the images is considerable since it shows the time distribution as well as the spatial (emission β and azimuthal δ angles) distribution of scattered and recoiled particles. Each window can be resolved into 255 time frames that can be as short as 16.3 ns each. The velocities (energies) of scattered and recoiled particles are analyzed by measuring their flight times from the sample to the MCP using a multiple-stop time-to-digital converter.

The Pt single crystals in the form of $1 \times 9 \text{ mm}$ disks were polished within 0.5° of the $[111]$ direction and cleaned by repeated cycles of 3 keV Ar^+ sputtering and annealing to 900°C . Annealing was accomplished by electron bombardment heating from behind the crystals. The surfaces were considered clean and well ordered when no impurity features were observed in the SARIS images and the LEED images exhibited sharp

(1×1) patterns. The samples were mounted on a conventional manipulator that provides reproducible rotation in both azimuthal δ and incident α angles to within $\pm 1^\circ$. The pulsed, mass-selected ion beam has a duoplasmatron ion source that produces beam spot sizes down to 1 mm² with energies variable over the range 3–25 keV and a final energy spread of <50 eV. A two step pulsing system produces pulsed beam widths <30 ns and an average beam current of 10–100 pA (0.1–1 μ A dc current before pulsing). Countdown circuitry permits pulse repetition rates over a range of 5–20 kHz.

The 64×64 pixel MCP is mounted on a triple-axis goniometer [16] so that it can be positioned at different angles relative to the sample surface. An important aspect needing to be addressed is the experimental determination of a specific scattering/recoiling angle θ_p corresponding to pixel p on the MCP (see Fig. 1). While mutual detector and sample alignment is not critical in blocking cone studies [3], precise TOF measurements require knowledge of the scattering/recoiling angles and the TOF path lengths for each specific angle θ_p . In order for the imaged data to be properly analyzed, the location on the MCP that corresponds to particle trajectories normal to detector (or θ_0 in

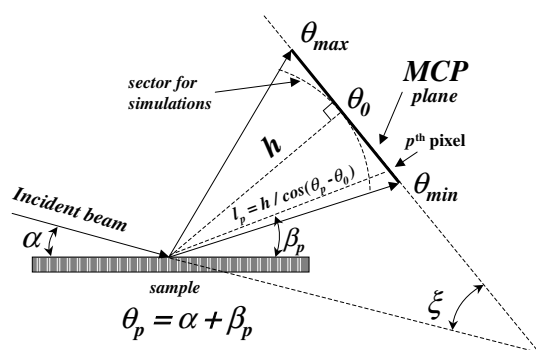


Fig. 1. Geometry of SARIS experiment and SARIC calculation. α —incidence angle, ξ —angle between incident beam and plane of MCP, β —variable emission angle, $\theta_p = \alpha + \beta_p$ —scattering/recoiling angle varying between (θ_{\min} and θ_{\max} and corresponding to pixel p on the MCP, and $h = 13$ cm—distance to the detector (at the position of the normal at θ_0) which is used for the SARIC calculation.

Fig. 1) from the point of ion impact on the sample and the maximum and minimum values of the scattering/recoiling angles (θ_{\max} , θ_{\min}) must be precisely defined. For this reason, a routine laser alignment procedure was developed to define these experimental parameters. This procedure was carried out before each experiment in which any parameters had been varied from their previous values. The “active angular window” of the MCP detector was calibrated by replacing the sample with a mini-electron gun.

The scattering angle θ in SARIS can be varied through 180°; the measurements presented herein are for one MCP position with $\theta_0 \approx 57^\circ$, $\theta_{\max} \approx 67.5^\circ$, and $\theta_{\min} \approx 48.5^\circ$. The in-plane scattering/recoiling geometry with incident angle $\alpha = 27^\circ$ along the $\langle 112 \rangle$ azimuth of the Pt(111) surface was used. This geometry was chosen due to its high sensitivity to the adsorption site position [17] at the (111) surface.

2.2. Computational methods

Ion trajectory simulations from the SARIC [8,9] program were used to calculate the angle-resolved energy distributions of scattered atoms and recoils. SARIC is based on the binary collision approximation [18,19], similar to that used in the well known program MARLOWE [7]. It describes the interactions between atoms and follows the trajectories of all scattered and recoiled atoms in three-dimensions, thereby capturing both in- and out-of-plane single and multiple collision events. It uses standard screening Coulomb potential functions to simulate the three-dimensional motions of atomic particles. The Ziegler–Biersack–Littmark universal potential [20] was used in these simulations. Other details are provided elsewhere [8,9]. Surface Debye temperatures, as estimated by Jackson [21], were used to generate the three-dimensional thermal vibrations of atoms around their equilibrium positions with rms amplitudes of 0.06 Å as in our previous work [17]. Calculations were performed for targets containing both one and four atomic layers in order to determine the sensitivity of the technique to the first atomic layer.

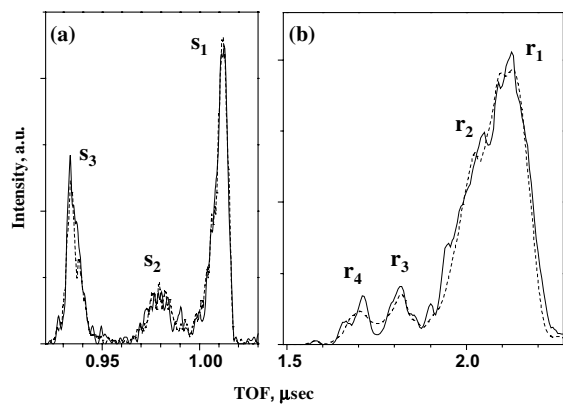


Fig. 2. Simulated TOF spectra for the Pt(111) target with 1 layer (---) and 4 layers (—) for the case of $\theta = 52^\circ$: (a) spectra of scattered Kr atoms and (b) spectra of recoiled Pt atoms. The main features can be separated into three scattering (s_1 – s_3) and (r_1 – r_4) peaks.

3. Results

3.1. Depth sensitivity

The contributions to the scattering and recoiling yields from different layers were calculated from SARIC for various angles. Fig. 2 shows typical scattering (a) and recoiling (b) spectra for a surface consisting of one layer (dashed line) and four layers (solid line) with $\theta = 52^\circ$. The similarity of these two simulated spectra confirms that the distributions of the scattered and recoiled particles are mainly determined by the first-layer atoms. The main features in Fig. 2 can be separated into three scattering (s_1 – s_3) and four recoiling (r_1 – r_4) peaks with explanations given below.

3.2. Contour plots of angular distributions

Experimental two-dimensional contour plots of the scattering and recoiling intensities as a function of the scattering and recoiling angles and flight times are shown in Fig. 3 as extracted from SARIS frame analysis. A horizontal cut through the figure gives an energy distribution at a fixed emission angle and a vertical cut gives an angular distribution at fixed energy (or fixed TOF).

The left side of Fig. 3 presents the experimental angular distribution of scattered Kr particles, while the right side consists of the distribution of recoiled

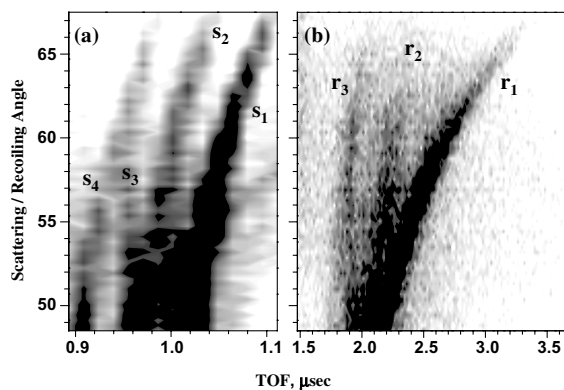


Fig. 3. Experimental SARIS two-dimensional contour plots of the (a) scattering and (b) recoiling intensities as a function of the scattering/recoiling angle and flight time for the Pt(111) surface. The number of detected trajectories increases from the white to the black color. The main features can be separated into four scattering (s_1 – s_4) and three recoiling (r_1 – r_3) traces.

Pt particles. Here we use the term ‘particles’ to represent scattered and recoiled atoms and ions. As in Fig. 2, the main features can be separated into scattering (s_1 – s_4) and recoiling (r_1 – r_3) traces. As will be shown later, s_1 and r_1 can be described as quasi-single scattering and recoiling collision events, while s_2 – s_3 and r_2 – r_3 include two or more large-angle collision events. s_4 is a small quasi-single scattering contribution from the ^{83}Kr isotope (with position affected by the value of T_0 in Eq. (7) below).

Similar angle versus TOF scattering and recoiling mapping distributions were obtained from the simulation by running sets of TOF spectral calculations (such as in Fig. 2) for the same range of exit angles (see Fig. 1) using half degree steps and the constant flight length $h = 13$ cm. The complete angle versus TOF scattering and recoiling mapping distribution can then be constructed by combining these partial spectra. The calculated contour plot distributions of the scattered and recoiled particles for a single layer target can also be separated into three scattering (s_1 – s_3) and four recoiling (r_1 – r_4) traces as shown in Fig. 4.

4. Separation of collision sequences and fractional yields

Classical kinematical analysis is particularly useful in studying the details of the scattering and

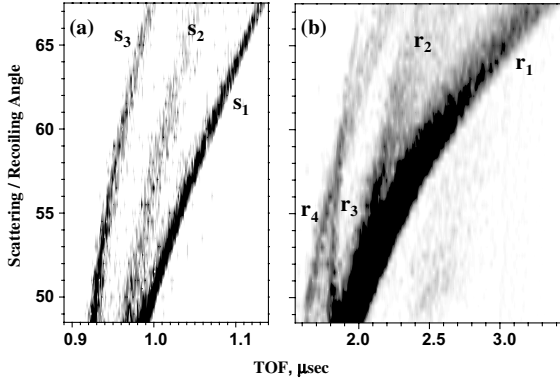


Fig. 4. Simulated SARIC two-dimensional contour plots similar to those of Fig. 3 for the Pt(111) surface consisting of a single atomic layer. The main features are the same as in Fig. 2.

recoiling events since the observed particles leave the surface as a result of individual primary impacts, the associated cascades are not complex, and the ejected atoms are mainly from the first layer. Here we compare the experimental data with the calculated dependencies from SARIC simulations and simplified collision kinematical equations.

The well known kinematical description of collisions [2,18,19] provides information about the final energies and scattering angles of interacting particles. The energies of scattered and recoiled atoms in an elastic collision can be determined from the conservation of energy and momentum as

$$E_S = E_0 \prod_i f_S(\theta_i) \quad (1)$$

and

$$E_R = E_0 \prod_{i,j} \{f_S(\theta_i) \times f_R(\theta_j)\}, \quad (2)$$

with

$$f_S(\theta_i) = \frac{\left(\cos(\theta_i) \pm \sqrt{\left(\frac{M_2}{M_1}\right)^2 - \sin^2(\theta_i)} \right)^2}{\left(1 + \frac{M_2}{M_1}\right)^2} \quad (3)$$

and

$$f_R(\theta_j) = \frac{4 \left(\frac{M_2}{M_1}\right) \cos^2(\theta_j)}{\left(1 + \frac{M_2}{M_1}\right)^2}, \quad (4)$$

where E_0 is the energy of the incident ion with mass M_1 , M_2 is the mass of a target atom which is initially at rest, $\theta_{i,j}$ are the partial scattering or recoiling angles, and $f_{S,R}$ is the fraction of energy transferred during the scattering or recoiling event. For in-plane geometry,

$$\sum_{i,j} \theta_{i,j} = \theta = \alpha + \beta, \quad (5)$$

where θ is the angle between the direction of the incident beam and the direction of the outgoing particle, α is the angle of incidence, and β is the emission angle. When the scattering/recoiling plane is not normal to the target surface, the partial angle is determined by

$$\cos \theta_i = \cos \alpha_i \cos \beta_i \cos \phi_i - \sin \alpha_i \sin \beta_i, \quad (6)$$

where α_i is the partial incident angle, β_i is the partial emission angle, and ϕ_i is the partial azimuthal angle. It is easy to see that for particles experiencing out-of-plane collisions, $\sum_{i,j} \theta_{i,j} > \theta$. When the energy and mass of the analyzed particles are known, the energy E of the particles is connected with the time-of-flight TOF_p corresponding to pixel p on the MCP (Fig. 1) and the measured flight time (T_M) by the relation

$$T_M = \text{TOF}_p + T_0 + \Delta, \quad \text{with } \text{TOF}_p = l_p \sqrt{\frac{M}{2E}}, \quad (7)$$

where M is the particle mass, l_p is the flight length, i.e. the distance between the target and pixel p on detector (see Fig. 1), T_0 is the time it takes the particle to travel between the pulsing aperture and the sample, and Δ is the fixed electronics delay.

Fig. 5 compares TOF distributions predicted by SARIC using corrected flight length l_p (solid circles) and measured by SARIS (open circles) with various curves from Eqs. (1) and (2). The definitions of the experimental and SARIC traces (r_1 – r_4 , s_1 – s_3) are the same as in Figs. 3 and 4. The experimental and calculated peak positions are very close to those of the theoretical binary collision curves that include a maximum of two collisions. The relevant processes are shown schematically in Fig. 5. Curves SS and DR correspond to processes s_1 and r_1 , respectively, defining positions for the energies of particles after a single collision. If

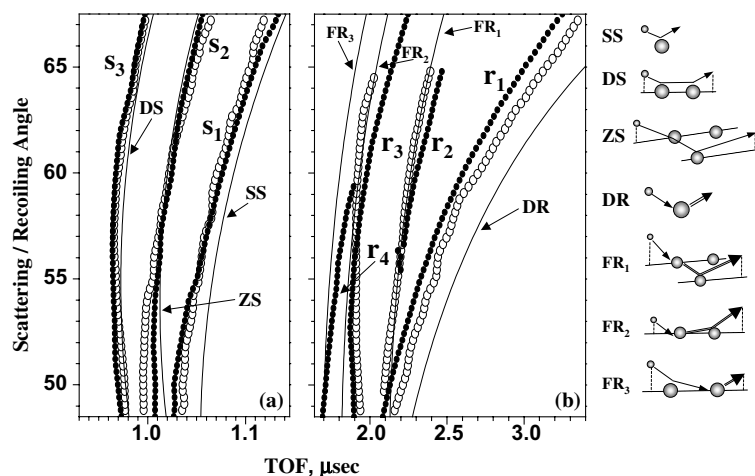


Fig. 5. Comparison of experimental results (○), SARIC calculations (●), and various curves obtained using Eqs. (1) and (2). The definitions of experimental and SARIC traces are the same as in Figs. 2–4. Seven observed collision sequences are shown schematically with explanations given in text.

several large impact parameter, or “quasi-single” collisions, with angles $\sim 1\text{--}2.5^\circ$ are included for incoming and outgoing particles, improved agreement between the SARIS/SARIC results can be obtained. The rest of the higher energy traces in Fig. 5 cannot result from a single binary collision event; at least two binary collisions are necessary to produce these traces. A more detailed understanding of such high energy events can be achieved if the actual trajectories of the scattered and recoiled particles are determined. Such trajectories have been extracted from the SARIC simulations. In-plane collisions can be defined as a double scattering process (DS) from atoms lying in a single row corresponding to trace s_3 . For recoil, a possible collision sequence is the following: a primary ion recoils a Pt atom which scatters off a second Pt atom in the same surface row (curve FR_2 or trace r_3). Curve FR_3 corresponds to a collision sequence in which Kr scatters parallel to the surface and then recoils a Pt atom. For out-of-plane collisions including atoms from two parallel rows, one can observe only fixed zigzag collisional events. From comparison of SARIS and SARIC results with curves from Eqs. (1) and (2), we find that only two angles are possible in zigzag collisions, i.e. $\sim 20^\circ$ (for ZS) and $\sim 22^\circ$ (for FR_1). These angles do not belong to any specific crystallo-

graphic directions and are most likely related to the nature of the screening function for a given collision pair.

Fig. 6 depicts the experimental and simulated intensity distributions extracted from Figs. 3 and 4. Comparison of Figs. 5 and 6 shows that the experimental and simulated spatial distributions are in quantitative agreement, however the experimental and simulated intensity distributions differ. This difference is more pronounced in Fig. 7, which shows the change in the intensity ratio of “single recoiling events” to “single scattering events” as a function of the scattering/recoiling angle. The ratio of differential cross-sections for binary recoiling and scattering collisions is included for comparison. This ratio was normalized by the coefficient

$$K = \frac{\cos \theta_{i,j}}{\sqrt{\left(\frac{M_2}{M_1}\right)^2 - \sin^2(\theta_{i,j})}}, \quad (8)$$

which relates the intensities in TOF and energy distributions as obtained by differentiating Eqs. (3) and (4). The difference between the theoretical values and SARIC calculations can appear for any of several reasons, of which the most important is the effect of thermal vibrations. This can be corroborated by SARIC data obtained using same

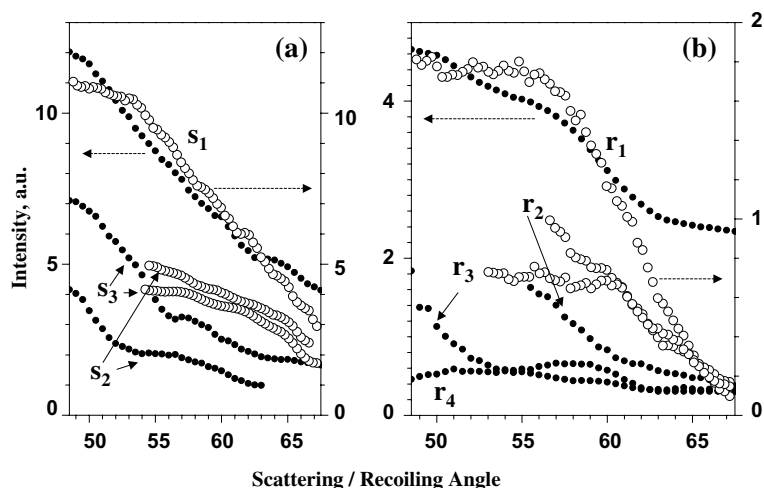


Fig. 6. Intensity dependencies of experimental (○) and simulated (●) scattering and recoiling traces from Figs. 3 and 4 as a function of scattering/recoiling angle.

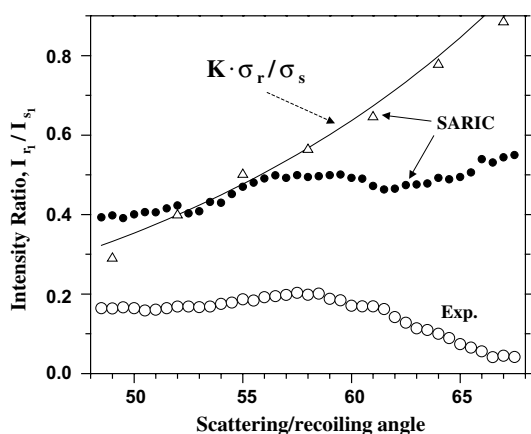


Fig. 7. Dependence of the “single recoiling” to “single scattering” intensity ratio r_1/s_1 on the scattering/recoiling angle: (○) experiment; (●) SARIC simulations for target with rms vibrational amplitude of 0.06 Å; (△) SARIC simulations for target without vibrations. The solid curve shows the scaled ratio of differential cross-sections for a binary collision.

target with no vibration (shown in Fig. 7 by open triangles). The width of the presented experimental peaks, the error in the angular function for the TOF distance, and the statistics in the calculated data do not allow us to draw any definite conclusions about inelastic losses or escape depths at this time. Nevertheless, the particles in the scattering and recoiling peaks must come from the first few

surface layers, otherwise there would not be agreement between the experimental peak positions and those of the binary collision model.

5. Discussion

5.1. Kinematics of the collisions

Our results show that angular distributions of scattering and recoiling particles can be simplified by using a kinematical description obtained from TOF versus angular traces. A combination of SARIS experiments and SARIC simulations provides a sensitive probe, which can yield, within experimental error, a conclusive description of the three-dimensional collision behavior of energetic atoms scattered from the first atomic layer of a surface. The results presented in Figs. 3 and 4 exhibit multiplex features in the scattering and recoiling angular traces. SARIS and SARIC provide a quantitative separation of these features in scattering and recoiling spectra and accurate analysis of the collision sequences.

Much research has focused on studying the scattering features in experimental spectra. For example, experimental energy spectra have been analyzed in terms of “quasi-single” peaks and

“quasi-double” shoulders [18]. Generally, better agreement between experiments and simulations can be achieved if the full three-dimensional nature of the collision is recognized. For example, computer simulations have been used to identify peaks due to “planar” and “zigzag” collision sequences [17,22]. These results support our conclusion about the kinematic nature of separation and description of the observed peaks and traces in Figs. 2(a)–5(a).

Although the first observation of direct recoils created in a single binary collision dates back to the mid sixties [23], the detailed investigation of fast recoils has been limited. An extensive review on recoils by keV ions from crystal and polycrystalline surfaces has been given by Eckstein [24]. Since the recoil cross-section at high energies is low and most of the recoils are neutral atoms, it was concluded that TOF would be the most sensitive detection means for recoil spectrometry because it detects both neutral and charged particles.

The investigation of recoils from single crystal surfaces by the group of Molchanov and Mashkova [13,19,25] have shown that the energy spectra of fast recoils manifest themselves as multiple peaks due to blocking effects and thermal vibrations of the surface atoms as well as instrumental effects such as beam spot size and detector aperture size. Such multippeak features have also been observed by other authors [17,26] who attributed the multiple peaks to deflected recoil processes, using the terms “deflected recoils” [26] or “surface recoils” [2,17]. These terms refer collectively to events such as those involving scattering of an atom subsequent to the initial recoil and those involving scattering of the projectile prior to the recoil collision. Our results unambiguously demonstrate that such multicollision sequences can be separated using a simple kinematical approach.

5.2. Detection efficiency

Although the TOF technique does not require knowledge of the neutralization probability, which is usually unknown in a particle surface collision, quantitative analysis of scattering and recoiling yields is complicated by the need for determination of the detector efficiency. The observed differences

between the experimental data and simulated values in Fig. 7 clearly illustrate this important point. Complete agreement is not expected here because the detection efficiency (DE) of scattered and recoiled particles is energy dependent in experiment, but constant in simulation. The behavior of the DE is non-linear with respect to a number of parameters. A review describing the DE of noble gas atoms is given by Tassoto and Watson (TW) [27].

If the energies of the scattered Kr atoms in our experiments are sufficiently high such that we can assume that the DE ϵ_{so} is constant for all measured angles, the resulting differences between SARIC simulations and experimental distributions in Fig. 7 provide the possibility of determining the DE for the lower energy recoiled Pt atoms. Fig. 8 shows the ratio of the experimental data to SARIC simulations from Fig. 7 plotted as a function of particle velocity (energy) of the Pt recoils. The relative DE at high velocities is found from $\epsilon^* = \epsilon_{ro}/\epsilon_{so}$, where ϵ_{ro} is the saturation value of DE for Pt recoiling atoms. The relatively low values of absolute efficiencies are quite surprising. The linear region of the dependence in Fig. 8 for Pt atoms with energy less than ~ 2.5 keV is also of great interest. Using the expression for the DE from (TW) [27], the

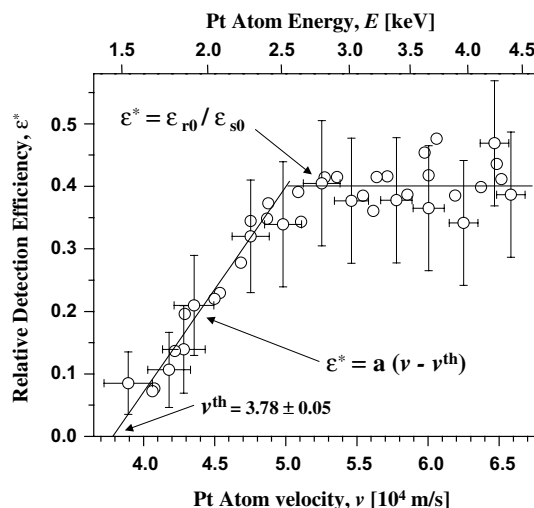


Fig. 8. Relative DE of Pt recoils with respect to Kr scattering versus the velocity (energy) of Pt atoms obtained by taking the ratio of experimental data to SARIC simulations from Fig. 7.

following form for the linear part of the ε^* dependency on velocity v is assumed

$$\varepsilon^* = a(v - v^{\text{th}}). \quad (9)$$

Here a is a constant and v^{th} is the threshold velocity that must be determined for a given particle. This value was previously determined [27,28] for a limited number of projectiles. The observed value $v^{\text{th}} = 3.78(5)$ for Pt recoils is intermediate between the values given by Ravon et al. [28] ($v^{\text{th}} = 4.18$) and (TW) [27] ($v^{\text{th}} = 2.71$), both values corresponding to Xe. We have not been able to find v^{th} values for heavier atoms for comparison. The demonstrated ability to distinguish between collision processes and study them quantitatively by properly taking the DE into account makes it possible to extend this method to other systems.

6. Conclusions

This study demonstrates that angle-resolved SARIS mapping combined with computer simulations is a valuable tool for characterization of scattering and recoiling events on a surface. The measurements allow identification of direct and indirect, i.e. multiple collision, scattering and recoiling particles in the energy distributions. Use of a large area MCP detector and TOF techniques decreases the collection time and increases the number of detected recoils above that of other designs. The scattering and recoiling contour map dependencies provide the kinematics of scattering and recoiling particles, their probability of being detected, and the probability for their occurrence in specific trajectories. Measured and simulated energy distributions agree quantitatively if the DE is taken into account. The value obtained for the threshold velocity, $v^{\text{th}} = 3.78(5) \times 10^4$ m/s, is in a good agreement with previous studies.

Acknowledgements

We are grateful to T. Ito for his assistance in computer analysis of the experimental results. This material is based on work supported by the National Science Foundation under grant no. CHE-

9986807. This work made use of the Center for Materials Chemistry (CMC-UH) Shared Experimental Facilities.

References

- [1] C. Kim, C. Hofner, A. Al-Bayati, J.W. Rabalais, *Rev. Sci. Instrum.* 69 (1998) 1676.
- [2] J.W. Rabalais, *Principles and Applications of Ion Scattering Spectrometry*, Wiley-Interscience, New York, 2002.
- [3] I.L. Bolotin, L. Houssiau, J.W. Rabalais, *J. Chem. Phys.* 112 (2000) 7181.
- [4] L. Houssiau, J.W. Rabalais, *Nucl. Instrum. Meth. B* 157 (1999) 274.
- [5] I. Vaquila, I.L. Bolotin, T. Ito, B.N. Makarenko, J.W. Rabalais, *Surf. Sci.* 496 (2002) 187.
- [6] J.W. Rabalais, *Am. Lab.* 33 (2001) 13.
- [7] M.T. Robinson, I.M. Torrens, *Phys. Rev. B* 9 (1974) 5008; M.T. Robinson, in: *Sputtering by particle Bombardment I*, in: R. Behrisch (Ed.), *Topics in Berlin Physics*, vol. 47, Springer, Berlin, 1981, pp. 73–144.
- [8] V. Bykov, C. Kim, M.M. Sung, K.J. Boyd, S.S. Todorov, J.W. Rabalais, *Nucl. Instrum. Meth. B* 114 (1996) 371.
- [9] M.M. Sung, V. Bykov, A. Al-Bayati, C. Kim, S.S. Todorov, J.W. Rabalais, *Scanning Microsc.* 9 (1995) 321.
- [10] T.T. Nuver, H. Rudolph, P.A. Zeijlmans van Emmichoven, A. Niehaus, *Nucl. Instrum. Meth. B* 164 (2000) 785; B. van Someren, T.T. Nuver, H. Rudolph, P.A. Zeijlmans van Emmichoven, I.F. Urazgil'din, A. Niehaus, *Surf. Sci.* 423 (1999) 276.
- [11] I. Reid, B.W. Farery, M.W. Thompson, *Nucl. Instrum. Meth.* 132 (1976) 317.
- [12] S.V. Teplov, T.L. Porter, C.S. Chang, U. Knipping, I.S.T. Tsong, *Phys. Rev. B* 38 (1988) 2225.
- [13] L.L. Balashova, A.M. Borisov, E.S. Mashkova, V.A. Molchanov, *Phys. Rev. A* 21 (1980) 1185.
- [14] Peabody Scientific, P.O. Box 2009, Peabody, MA 01960.
- [15] C. Kim, A. Al-Bayati, J.W. Rabalais, *Rev. Sci. Instrum.* 69 (1998) 1289.
- [16] J. Yao, C. Kim, J.W. Rabalais, *Rev. Sci. Instrum.* 69 (1998) 306.
- [17] I.L. Bolotin, A. Kutana, B. Makarenko, J.W. Rabalais, *Surf. Sci.* 472 (2001) 205.
- [18] E.S. Parilis, L.M. Kishinevsky, N.Yu. Turaev, B.E. Baklitzky, F.F. Umarov, V.Kh. Verleger, I.S. Bitensky, *Atomic Collisions on Solids*, North-Holland, New York, 1993.
- [19] E.S. Mashkova, V.A. Molchanov, *Medium-Energy Ion Reflection From Solids*, North-Holland, Amsterdam, 1985.
- [20] J.F. Zeigler, J.P. Biersack, U. Littmark, in: J.F. Ziegler (Ed.), *The Stopping and Range of Ions in Solids*, Pergamon Press, NY, 1985.
- [21] D.P. Jackson, *Sur. Sci.* 43 (1974) 431.
- [22] D.S. Karpuzov, E.V. Alonzo, R.P. Walker, D.G. Armour, D.J. Martin, *Surf. Sci.* 129 (1983) L271.
- [23] S.D. Datz, C. Snoek, *Phys. Rev. A* 134 (1964) 347.

- [24] W. Eckstein, Nucl. Instrum. Meth. Phys. Res. B 27 (1987) 78.
- [25] L.L. Balashova, A.M. Borisov, E.S. Mashkova, V.A. Molchanov, Surf. Sci. 80 (1979) 573; Surf. Sci. 77 (1978) L643; A.M. Borisov, A.I. Dodonov, V.A. Molchanov, Radiat. Eff. 80 (1984) 105.
- [26] D.J. O'Connor, Surf. Sci. 173 (1986) 593; D.J. O'Connor, R.J. MacDonald, W. Eckstein, P.R. Higginbottom, Nucl. Instrum. Meth. Phys. Res. B 13 (1986) 235.
- [27] M. Tassoto, P.R. Watson, Rev. Sci. Instrum. 71 (2000) 2704.
- [28] J.P. Ravon, Nucl. Instrum. Meth. Phys. Res. 211 (1983) 7.